

Cite this: DOI: 10.1039/xxxxxxxxxx

Supplementary Information: Deep Indentation and Puncture of a Rigid Cylinder Inserted into a Soft Solid

Christopher W. Barney,^a Chao Chen,^a and Alfred J. Crosby^{*a}

Received Date
Accepted Date

DOI: 10.1039/xxxxxxxxxx

www.rsc.org/journalname

1 Supplementary Videos

The supplementary videos associated with this paper are listed below.

- Supplementary Video SV1_1: Plot of the raw video data overlaid with the force data gathered via load cell.
- Supplementary Video SV1_2: Overlay of the displacement fields measured on each frame via the PIV ImageJ plugin of Tseng et al.¹
- Supplementary Video SV1_3: Overlay of the grid points ($X_{eul} = 128$) that define the Lagrangian mesh used to calculate strains.
- Supplementary Video SV1_4: Overlay of $-\epsilon_{22}$.
- Supplementary Video SV1_5: Overlay of $|\epsilon_{12}|$.
- Supplementary Video SV1_6: Overlay of $|\sigma_{22}/E|$.
- Supplementary Video SV1_7: Overlaid videos showing the removal process for points that cross onto the indenter.
- Supplementary Video SV1_8: Overlay of ϵ_{11} .
- Supplementary Video SV1_9: Overlay of I_1 .
- Supplementary Video SV1_10: Overlay of the grid points ($X_{eul} = 96$) that does not display a significant increase in data quality when compared to Supplementary video SV1_3.
- Supplementary Video SV1_11: Overlay of $|\Delta\sigma_{22}/E|$.
- Supplementary Video SV1_12: Overlay of $|\Delta\epsilon_{22}|$.

2 Raw Data

A schematic of the experimental setup and plots of the raw data are shown in Figure S1. The force versus displacement plot shown in Figure S1b displays several distinct features that occur at different penetration depths and are identified by red circles. Circle (i) shows the initial elastic loading region, where the deformation does not permanently damage the material. At larger indentation depths, this regime has been shown previously to scale with the square of displacement and can be fit with a single constant k^*E where k^* is an empirical constant typically on the order of about 0.3.² Circle (ii) highlights the puncture point at the end of the elastic loading regime. This end is identified by a drop in the force that indicates a noncontinuous change in the contact stiffness due to the nucleation of a macroscopic crack. Similar drops in force are observed between Circles (ii-iii), which indicate the buildup and release of strain energy as the crack propagates. Circle (iii) marks the start of the retraction regime, where the indenter is removed from the sample. Circle (iv) shows a point in the retraction, where the indenter has left behind a macroscopic defect along which the indenter slides before exiting the material.

To demonstrate the generality of the reported results, we provide a comparison between the force-displacement relationship for the material used here and force-displacement relationships from materials cured without the additional steps to include optical markers for DIC. We present these force-displacement measurements in a normalized format, where force and displacement are normalized by the corresponding critical value recorded when puncture is initiated. This normalized format is chosen since the elastomers have slightly different cure histories and composition. The unmarked samples consisted of 20:1 PDMS cured overnight at 70°C. Despite the differences in composition and cure conditions, the agreement of these curves shows that the experiment reported here for DIC is representative of a typical sample up to the point of puncture. After the point of puncture, the force displacement profile varies, as typical for all materials, as this data and the corresponding strain distribution depend upon the exact crack path and shape, which are functions of the geometry, ma-

^a Polymer Science and Engineering Department, University of Massachusetts, 120 Governors Drive, Amherst, MA, 01003, USA. Fax: +1 413 545 0082; Tel: +1 423 577 1313; E-mail: acrosby@umass.edu

terials properties, and materials structure and defects.^{3–5} While DIC continues to work after the puncture point, our results in this regime are not representative every possible crack path and shape that can be experienced in post-puncture fracture processes.

3 DIC Process and Selection of Reasonable Parameters

The DIC process consisted of four steps. The first step was to collect the raw data shown in Figure S1. Figure S1 shows a) a sketch of the experimental setup b-c) examples of the raw displacement, time, and force data gathered during the experiment as well as images showing the deep indentation and puncture process. This step is shown in Supplementary Video SV1_1.

The second step in the DIC process was to analyze the raw data using the PIV ImageJ plugin developed by Tseng et al.¹ The PIV step of the DIC analysis has several input parameters such as the interrogation window size, search window size, and vector spacing. The interrogation window size X_{eul} describes the size of the square window on the first frame used to identify distinguishing features. The search window size is the size of the window on the following frame where distinguishing features are correlated to those on the initial frame and is set to $2X_{eul}$. The vector spacing gives the spacing between the centers of each interrogation window on the frame and is set to $X_{eul}/2$. Setting the ratio between these quantities is convenient as it collapses three input parameters down to one. A value of $X_{eul} = 128$ was employed when analyzing the data presented in the main text. Examination of different input parameters is possible after the third DIC step. In addition to window size and spacing, the PIV plugin uses a correlation threshold value that ranges from -1 (no correlation) to 1 (perfect correlation). The default value of 0.6 was used when analyzing data. This threshold sets the correlation value below which the local displacements are not directly calculated and are instead interpolated from the surrounding data points. An example of this step is shown in Supplementary Video SV1_2.

The maximum frame-to-frame displacement from indenter speed (1 mm/s), resolution (35 pixels/mm), and acquisition rate (15.4 fps), giving an estimated displacement of approximately 2.3 pixels per frame. This value is higher as the material recoils during the puncture process; however, 2.3 pixels is smaller than our smallest interrogation window. The PIV plugin does not allow a search window that is smaller than the interrogation window. This limitation means that setting this window to a constant value across all cases would mean setting it extremely large for small values of X_{eul} . Instead, the search window is scaled with the interrogation window so that each scan is through the same relative area. The factor of two was set through a suggestion for a reasonable value from the instructions for the PIV plugin.

The third step consists of converting the Eulerian grid of frame-by-frame displacements to a Lagrangian mesh of points. This was done by taking the displacement field and interpolating it to make a continuous function. Then a grid of points was introduced on the first frame of interest in the video (frame 222). The location of each of these grid points was then updated on every remaining frame in the video using the interpolated displacement

field function. Those points that cross over the indenter itself were removed from the mesh. This removal process is shown in Supplementary Video SV1_7 as the boundaries of the probe were identified as that of the largest contiguous dark region on the frame after thresholding. Thresholding was performed using the `graythresh` command which employs Otsu's method to identify the threshold level.⁶

A full loading and unloading cycle of the deep indentation and puncture process was performed and comparing the first and final frames of the video show that there was no observable residual strain left at the end of deformation. This choice is useful in that it provides a metric for quantifying the error in using an input value of $X_{eul} = 128$ for the DIC process as any point that is introduced in the system that is not removed from the mesh during the fracture process should return to its initial position. A plot of the cumulative frequency against the absolute value of the difference between the initial and final position of points is shown in Figure S3. This plot shows a small span between the values of X_{eul} , which favors larger values. This preference towards larger values of X_{eul} is likely related to the relative size and spacing of the optical markers. The optical markers have a diameter of 35 pixels and were spaced on a square grid with a 70 pixel center-to-center spacing. This spacing appears to correlate with the observation that $X_{eul} > 64$ produces less error. This observation suggests that the choice of $X_{eul} = 128$ is reasonable as it fully spans two optical markers (105 pixels). For comparison, the grid of points generated when $X_{eul} = 96$ has been included in Supplementary Video SV1_10 and does not show a significant increase in data quality.

The final step in the DIC process was converting the Lagrangian mesh into a mapping of the stress and strain fields. This process was covered in Sections 3-4 of the main text and it consisted of calculating the deformation gradient under an assumption of axisymmetry in order to find the Green strain. In addition to the mappings shown in Figure 4, overlays of ϵ_{11} and I_1 are shown in Supplementary Videos SV1_8 and SV1_9, respectively.

References

- 1 Q. Tseng, E. Duchemin-Pelletier, A. Deshiere, M. Balland, H. Guillou, O. Filhol and M. Thery, *Proceedings of the National Academy of Sciences*, 2012, **109**, 1506–1511.
- 2 S. Fakhouri, S. B. Hutchens and A. J. Crosby, *Soft matter*, 2015, **11**, 4723–4730.
- 3 A. Stevenson and K. Ab Malek, *Rubber Chemistry and Technology*, 1994, **67**, 743–760.
- 4 O. a. Shergold and N. a. Fleck, *Proceedings of the Royal Society A: Mathematical, Physical and Engineering Sciences*, 2004, **460**, 3037–3058.
- 5 W.-c. Lin, K. J. Otim, J. L. Lenhart, P. J. Cole and K. R. Shull, *Journal of Materials Research*, 2009, **24**, 957–965.
- 6 N. Otsu, *IEEE Transactions on Systems, Man, and Cybernetics*, 1979, **SMC-9**, 62–66.

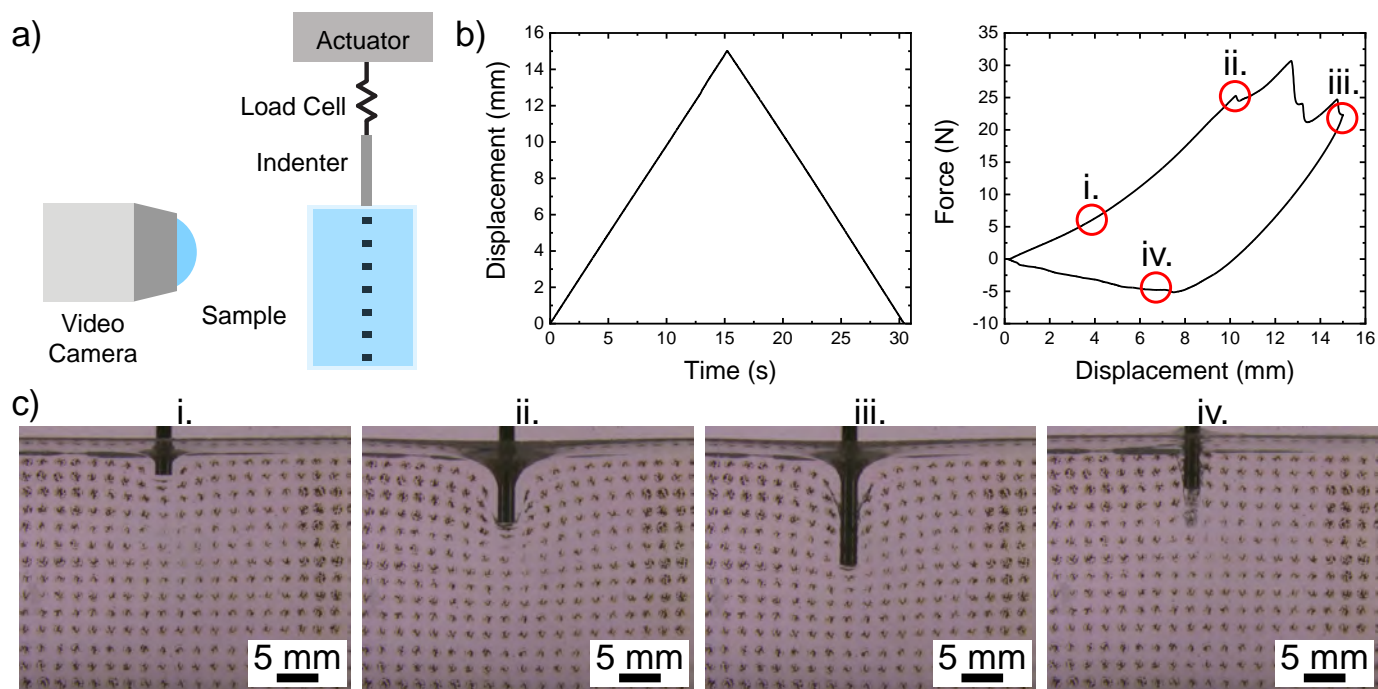


Fig. S1 a) a sketch of the experimental setup. b) The raw displacement, time, and force data gathered during the experiment. c) Images showing the deep indentation and puncture process. synchronized to the time points marked in b).

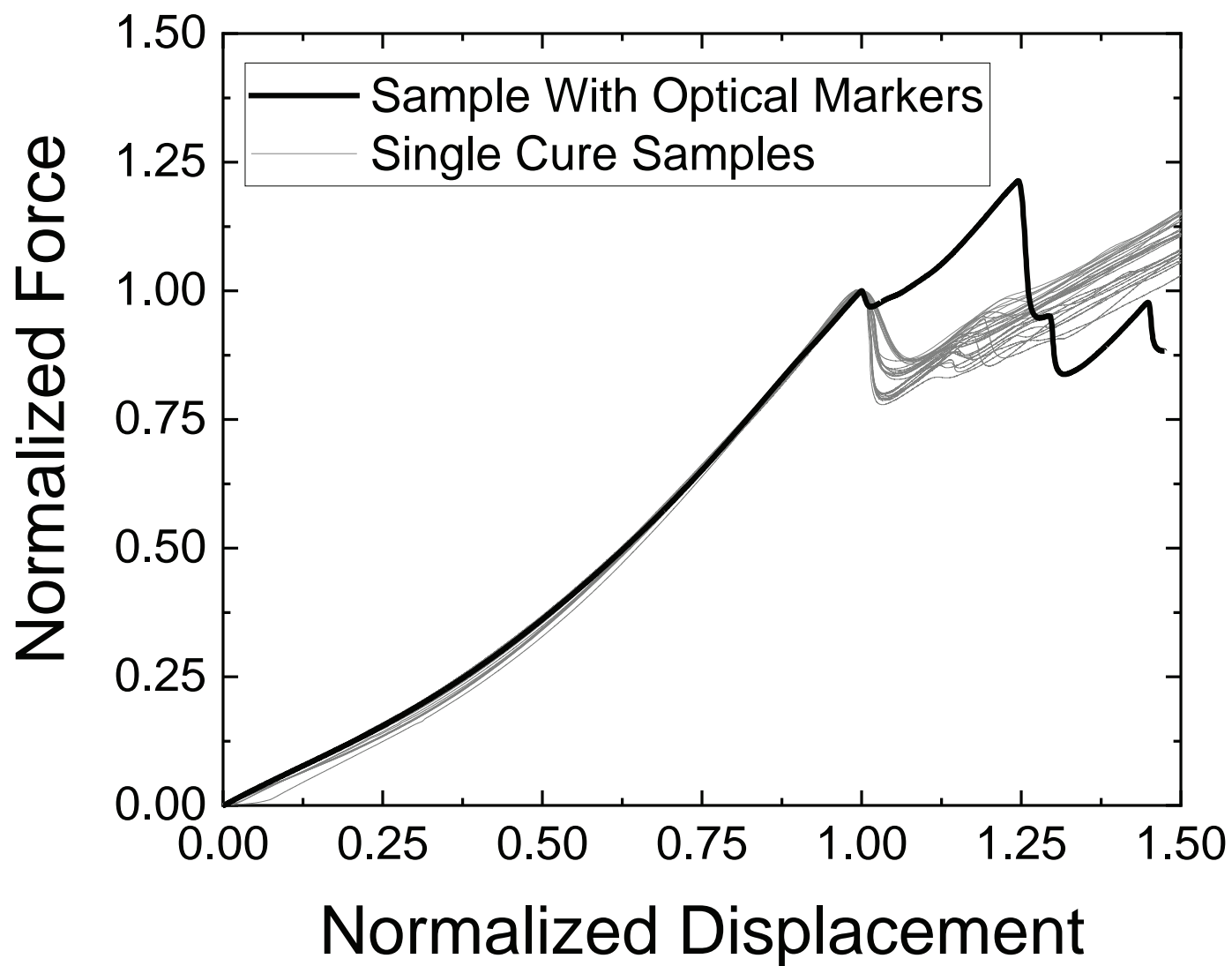


Fig. S2 Plot of the force vs displacement, normalized by the critical value at puncture, profile for the multi-step cured sample analyzed in this work as well as some single cure samples. The single cure samples includes 10 runs with displacement speeds at 0.1, 1, and 10 mm/s. The agreement of these curves shows that our results are general up to the point of puncture.

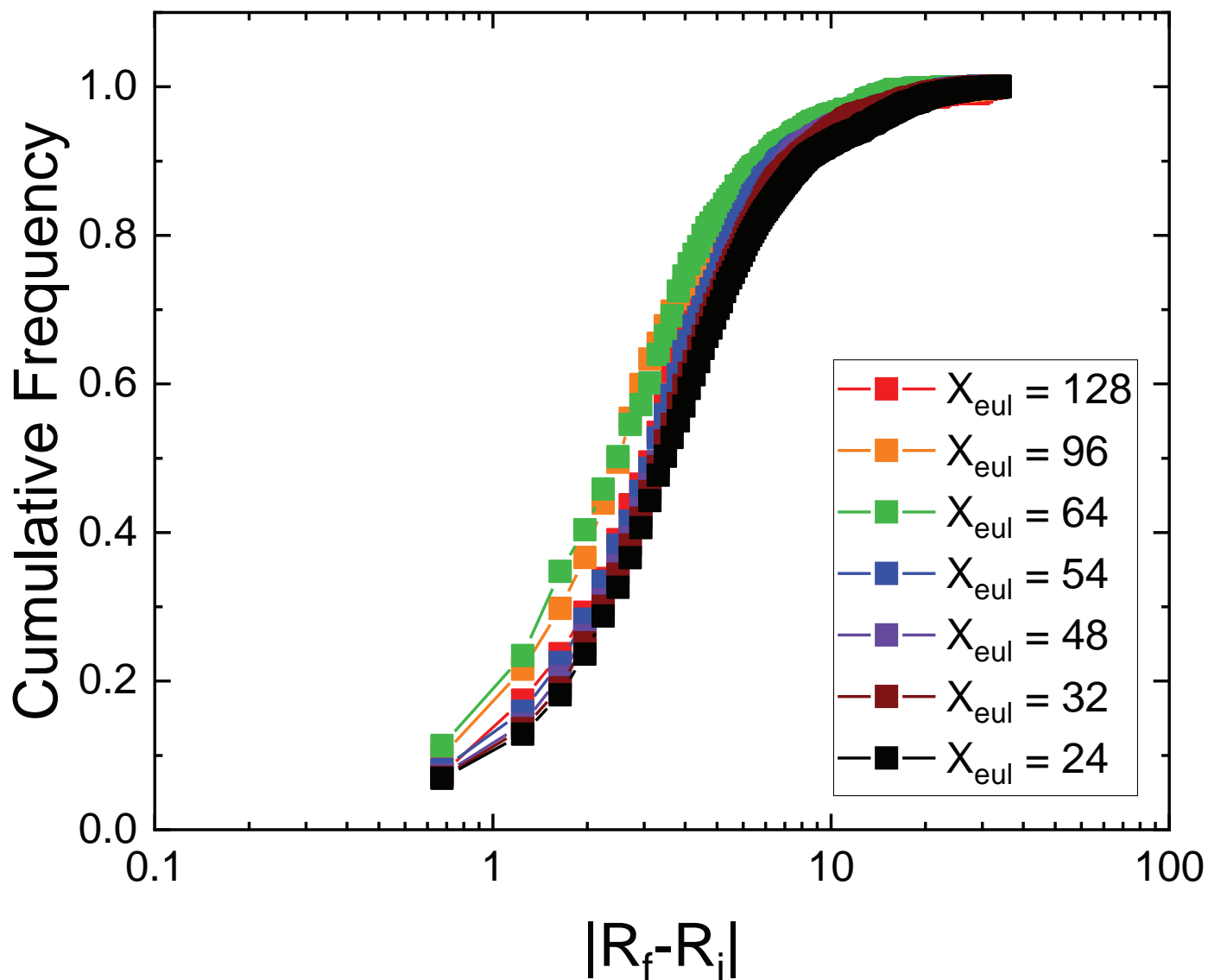


Fig. S3 Plot of cumulative frequency against the difference between the initial and final position of points normalized for different values of X_{eul} given in pixels. Images were captured at a resolution of 35 pixels per mm.

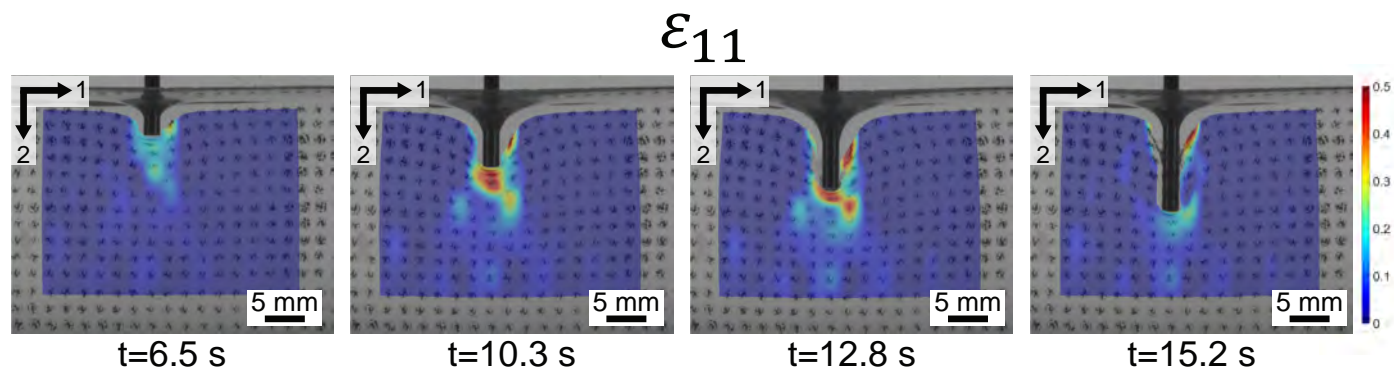


Fig. S4 Image of the outward strain field around the indenter at different time points up to the point of retraction.

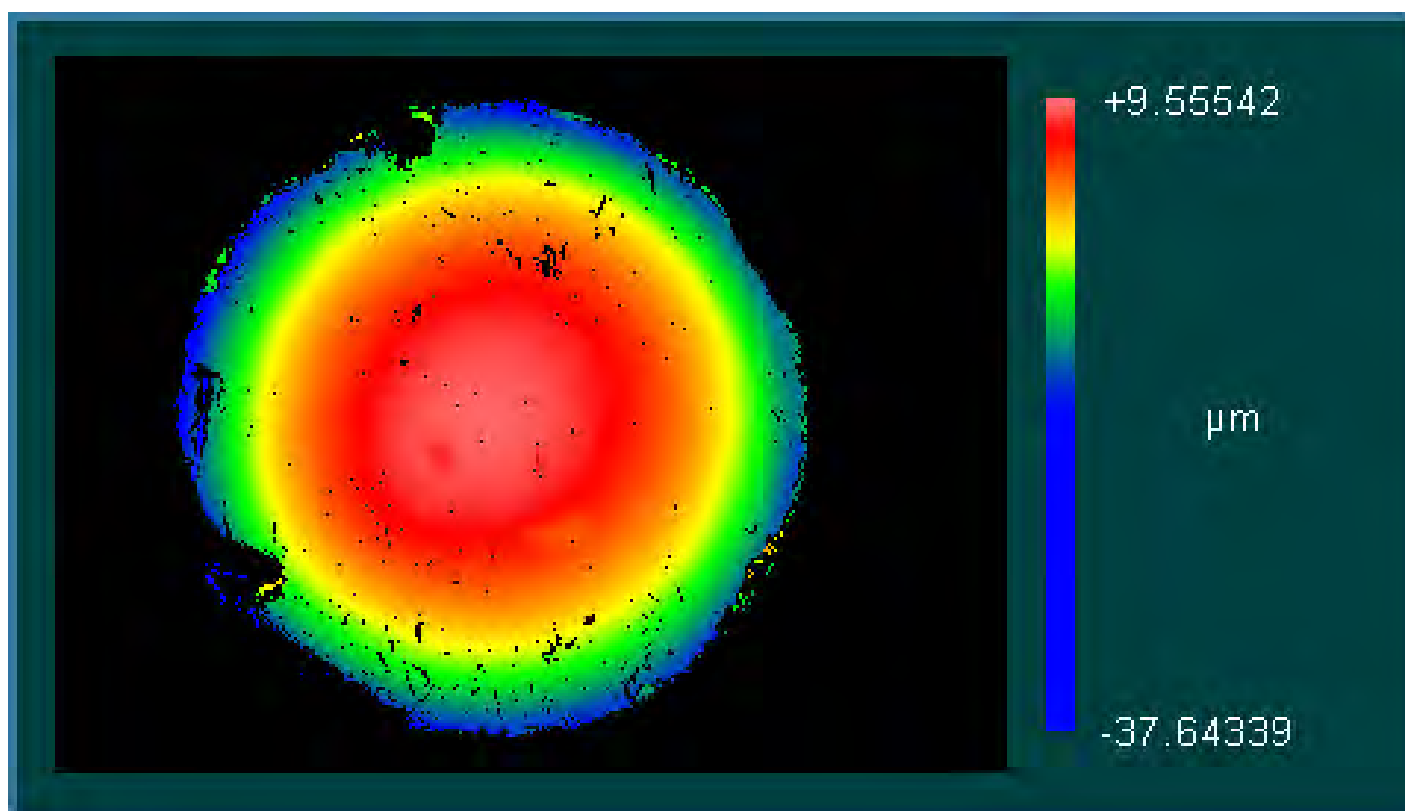


Fig. S5 Profile of the probe tip captured via optical profilometry. This measurement results in an estimated root mean square roughness value of 6.35 μm .